SYSTEMS BIOLOGY

Reverse control of biological networks to restore phenotype landscapes

Insoo Jung, Corbin Hopper, Seong-Hoon Jang, Hyunsoo Yeo, Kwang-Hyun Cho*

Biological systems consist of genetic elements and their regulatory interactions, forming networks that maintain life. However, accumulated alterations such as DNA damage can distort biological behavior, leading to undesirable responses to stimulus. This raises the question of whether we can restore their nominal stimulus-response relationships. Current control approaches tend to enforce a single desired response rather than restore the proper capacity for variable responses to different stimulus. Here, we present an algebraic reverse control (ARC) framework for reversion of altered biological networks. ARC leverages matrix operations to quantify the phenotype landscape of the altered network and identifies reverse control targets for recovering the phenotype landscape of a nominal network. ARC is scalable to large Boolean networks and identifies effective control targets to restore biological behavior.

INTRODUCTION

Biological systems have evolved to produce appropriate responses for each external stimulus from their environment to survive. These responses codify the nominal dynamical behavior, which is essential for living organisms to maintain their life. However, this nominal behavior can be distorted by accumulated alterations, such as DNA damage or epigenetic changes, leading to undesirable stimulus-response relationships. For instance, a cancer cell may exhibit uncontrolled proliferation irrespective of external growth factor signals or apoptotic signals (*1*–*4*). A key question arises as to whether we can control these altered biological systems to recover their nominal dynamical behavior and, if so, how we can achieve this control (*5*).

To address these questions, we investigate biological systems to analyze the recovery of nominal dynamical behavior. Biological systems are composed of molecular components and complex regulatory interactions between them. These systems and their dynamics can be represented by complex molecular regulatory networks. In particular, we use the Boolean network model, which despite being one of the simplest mathematical models, still effectively captures the essential dynamics of complex biological systems (*6*–*8*). A Boolean network model is a logical dynamic model with binary node states, where each node represents the activity of a molecular component [high (1) or low (0)]. Regulatory interactions between molecular components are represented by logical links connecting the nodes, without the use of kinetic parameters. The network state, defined by the collection of node states, eventually converges to a steady-state known as an attractor, while the basin of an attractor is defined as the set of network states that converge to the same attractor.

From a systems perspective, the steady-state value of the output nodes within each attractor can be defined as the phenotype of that attractor, which corresponds to the phenotype of that biological system. Therefore, the phenotype landscape, comprising all phenotypes of attractors and their respective basins, contains the network state sets grouped by their phenotype after convergence. The landscape is crucial for understanding system behavior, as it encodes both the relative likelihood of each phenotype and the internal node states that influence phenotypic changes in response to epigenetic modifications, mutations, and external pathways outside the model. However, the nominal phenotype landscape can be distorted by accumulated alterations, in turn changing the resulting behavior of the system. In this study, we define the reversion of dynamic behavior as the recovery of the nominal phenotype landscape (*5*).

Recently, the control of Boolean networks has garnered considerable attention (*9*–*12*). Most existing control methods aim for convergence to a single desired attractor or phenotype by perturbing certain network nodes to fixed values (*13*–*16*). Several methods do focus on reverting the phenotype but do not consider reversion of the landscape itself (*17*–*22*). On the other hand, to revert the entire phenotype landscape, it is crucial to restore the phenotypes of all attractors and their corresponding basins, rather than merely driving all or some basins to a single desired attractor. Consequently, it is necessary to identify the phenotype of the attractor that corresponds to each network state for effective reversion of the phenotype landscape. However, currently available control methods for complex networks do not investigate which attractors and their phenotypes correspond to which network states, making them unsuitable for the reversion of the entire phenotype landscape. Thus, phenotype landscape reversion presents a challenging problem for the reverse control of altered biological networks.

A common method for precisely analyzing the dynamics of every Boolean network state is the semitensor product (STP) approach (*23*–*28*). This method calculates linear operator matrices algebraically to represent the state transition graph (STG) of a Boolean network. However, among studies using STP, including those focusing on controlling output nodes of Boolean networks (*18*, *19*), no method currently exists to address reversion to a nominal phenotype landscape that considers the corresponding basins. Moreover, STP is critically limited by its high computational complexity with respect to network size and requires a novel approximation to extend its utility to large networks. Several non-STP methods allow for updating states in reverse, which could theoretically be used to find the phenotype basin but require similar complexity to brute-force simulation to characterize the entire landscape (*29*, *30*).

In this study, we present an algebraic reverse control (ARC) framework to systematically analyze the distortion degree between the

Laboratory for Systems Biology and Bio-inspired Engineering, Department of Bio and Brain Engineering, Korea Advanced Institute of Science and Technology (KAIST), 291 Daehak-ro, Yuseong-gu, Daejeon 34141, Republic of Korea.
*Corresponding author. Email: ckh@kaist.ac.kr

nominal and altered phenotype landscape and identify control targets to recover nominal phenotype landscapes. We first develop an exact ARC framework that is suitable from small networks. We leverage linear operator matrices based on the STP, which represent nonlinear state transitions of a Boolean network, to compute the attractors and their basins of attraction through eigen decomposition of linear operator matrices. Furthermore, by examining these attractors and their basins, we quantitatively measure the degree of distortion between the nominal and altered phenotype landscapes. We define the reverse control score such that a low degree of distortion in the controlled phenotype landscape yields a high control score. Last, we propose a reverse control strategy that maximizes the reverse control score and demonstrate its effectiveness by identifying a reverse control target of a Boolean epithelial growth factor signaling network.

We then develop an approximate ARC framework to overcome the computational limitations of STP for large networks. A first-order Taylor approximation of the Boolean update logic is developed with high accuracy, which maintains the linearity required to calculate average basin states, unlike other approximations of similar complexity (*31*). We examine the accuracy of the proposed approximation with various biological Boolean networks and demonstrate its utility through an example of reverting abnormal T cell overactivation on a large Boolean network. This suggests that the approximate ARC framework can restore the capacity for variable response that is characteristic of biological systems. The combination of a mathematically comprehensive framework and a practically efficient approximation implies a wide range of applications for reverse control of phenotype landscapes.

RESULTS

Overview of phenotype landscape reversion

Biological systems process external stimuli and generate appropriate responses through signal propagation within a complex molecular network (Fig. 1A). Here, we introduce Boolean network modeling to systematically analyze the dynamic behavior of these networks. In general, input nodes receive external stimuli, internal nodes propagate those stimuli, and output nodes determine an appropriate biological phenotype based on the propagated signals (Fig. 1B). During propagation, node state values are updated synchronously until the network reaches a steady state known as an attractor. The output node state values at each attractor can define the phenotype (Fig. 1C).

The attractor landscape can be represented by the STG, which includes all possible 2^n network states and transitions between them. In synchronous dynamics, each weakly connected component of the STG represents a basin that converges to the same attractor, and each strongly connected component of the STG represents one such attractor (Fig. 1D). The correspondence between the basins and their attractors is referred to as the attractor landscape. In the attractor landscape, basins are separated by the states of the input nodes and possibly by certain internal nodes states as well. The correspondence between the basins and their phenotypes is referred to as the phenotype landscape. When specific input node states are provided, they typically determine the phenotype. However, certain input node values do not uniquely determine the phenotype due to variations in their internal states (Fig. 1E).

If a node is fixed due to an alteration, the phenotype landscape can be distorted so that it no longer exhibits the nominal phenotype at each basin. In Boolean networks, a node can be fixed to 1 through a gain-of-function (GoF) alteration or fixed to 0 through a loss-of-function (LoF) alteration. A distorted phenotype landscape results in mismatches between the basin and the output node values of the reached attractor (Fig. 1, F and G). For instance, due to an alteration, basin 1 fails to converge to attractor 1 and instead converges to attractor 2, resulting in phenotype distortion. Similarly, basin 5 fails to converge to attractor 5 and instead converges to attractor 4, leading to distorted phenotypes.

To address these distortions, we define "reverse control" of the phenotype landscape as restoring the nominal phenotypes for each basin by perturbing an internal node in the Boolean network (Fig. 1, H and I). In contrast, existing control approaches aim to drive the network to a single attractor or phenotype. In the example, the reverse control restores the attractors and their basins to be nearly identical to those of the nominal landscape, showing that reversion of the phenotype landscape can be approximately achieved.

Identifying reverse control targets for phenotype landscape reversion

We developed an ARC framework for quantifying the distortion degree between the nominal and altered phenotype landscapes to identify potential reverse control targets. For small Boolean networks with up to 20 nodes, we presented an exact ARC framework based on the STP approach. For a given Boolean network, we first calculate the exact basin states through eigen decomposition of the transpose of the STP transition matrix. For each calculated basin, we compute its corresponding attractor and phenotype by consecutively multiplying the STP transition matrix under nominal, altered, and controlled conditions. We then measure the distortion degree between the nominal phenotype landscape and the altered or controlled phenotype landscape by comparing the reached phenotype for each basin after convergence under various conditions. The control target is selected as the one that minimizes the distortion degree. To illustrate our framework, we analyzed a toy Boolean network that consists of one input node, two internal nodes, and one output node, which are respectively depicted in blue, green, and yellow. Applying our algorithm under the GoF alteration of node Y, we identified the inhibition of node X as the optimal reverse control target (Fig. 2A and Methods).

For large Boolean networks with more than 20 nodes, we developed an approximate ARC framework. Our approximated approach uses a first-order Taylor approximation to overcome the exponential complexity of the STP approach. This converts Boolean update functions into linear update equations to approximate the forward and backward state transition matrices. First, we calculate the approximated average basin states through backward state transitions from given major attractors identified by simulation with random initial states. Then, for each approximated average basin state, we compute its corresponding attractor and phenotype by consecutively multiplying the approximated forward state transition matrix under nominal, altered, and controlled conditions. As in the exact ARC framework, we measure distortion degrees and define the reverse control target as the one that maximizes the reverse control score (Fig. 2B and Methods).

Efficiency of phenotype landscape reversion

To assess the efficacy of the ARC framework, we first evaluate the accuracy of the approximate ARC framework on biological networks with respect to its estimation of the phenotype landscape. To do so,

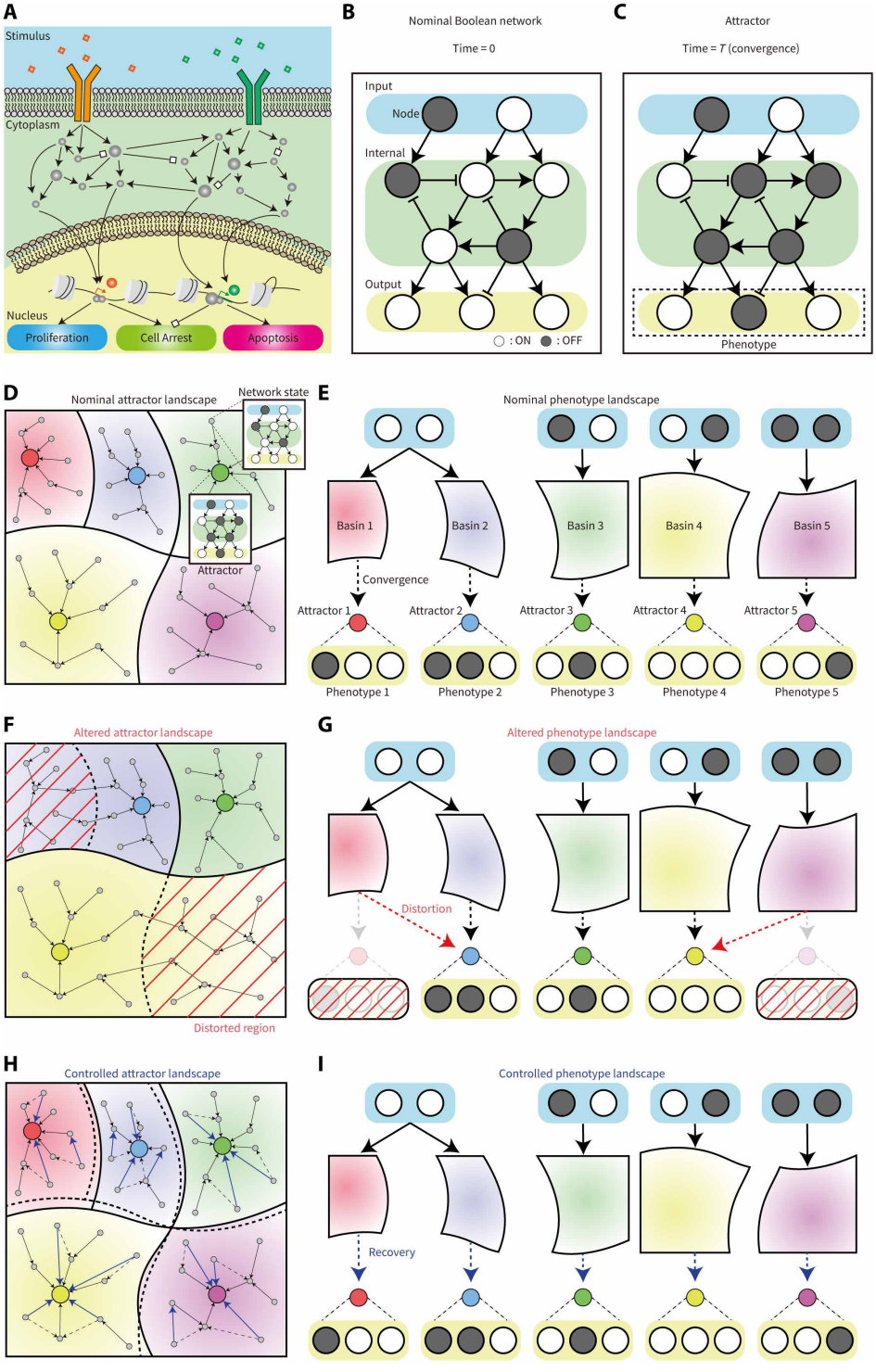

Fig. 1. Phenotype landscape reversion. (**A**) Signaling pathway system within a cell. The cell receives external stimulus at receptors, and the signals propagate into the nucleus to produce appropriate responses. (**B**) Representation of a biological system as a Boolean network. White nodes represent high expression levels ("ON"), while black nodes represent low expression levels ("OFF"). (**C**) Steady state of a Boolean network for a given input signal. The output node states determine the phenotype of the attractor. (**D**) Attractor landscape of a Boolean network represented on the STG. Each circle is a network state, with arrows representing transitions between states. There are five attractors (colored circles) and their corresponding basins (colored area). (**E**) Phenotype landscape of a Boolean network. Each of the five basins converges to a corresponding attractor and produces a distinct phenotype. (**F**) Altered attractor landscape of a Boolean network. A distorted region, defined as states with mismatched phenotypes, arises due to alteration. (**G**) Altered phenotype landscape of a Boolean network. (**H**) Recovered attractor landscape of a Boolean network. The attractors and their basins are restored to be nearly identical to those of the nominal landscape through reverse control. (**I**) Recovered phenotype landscape of a Boolean network.

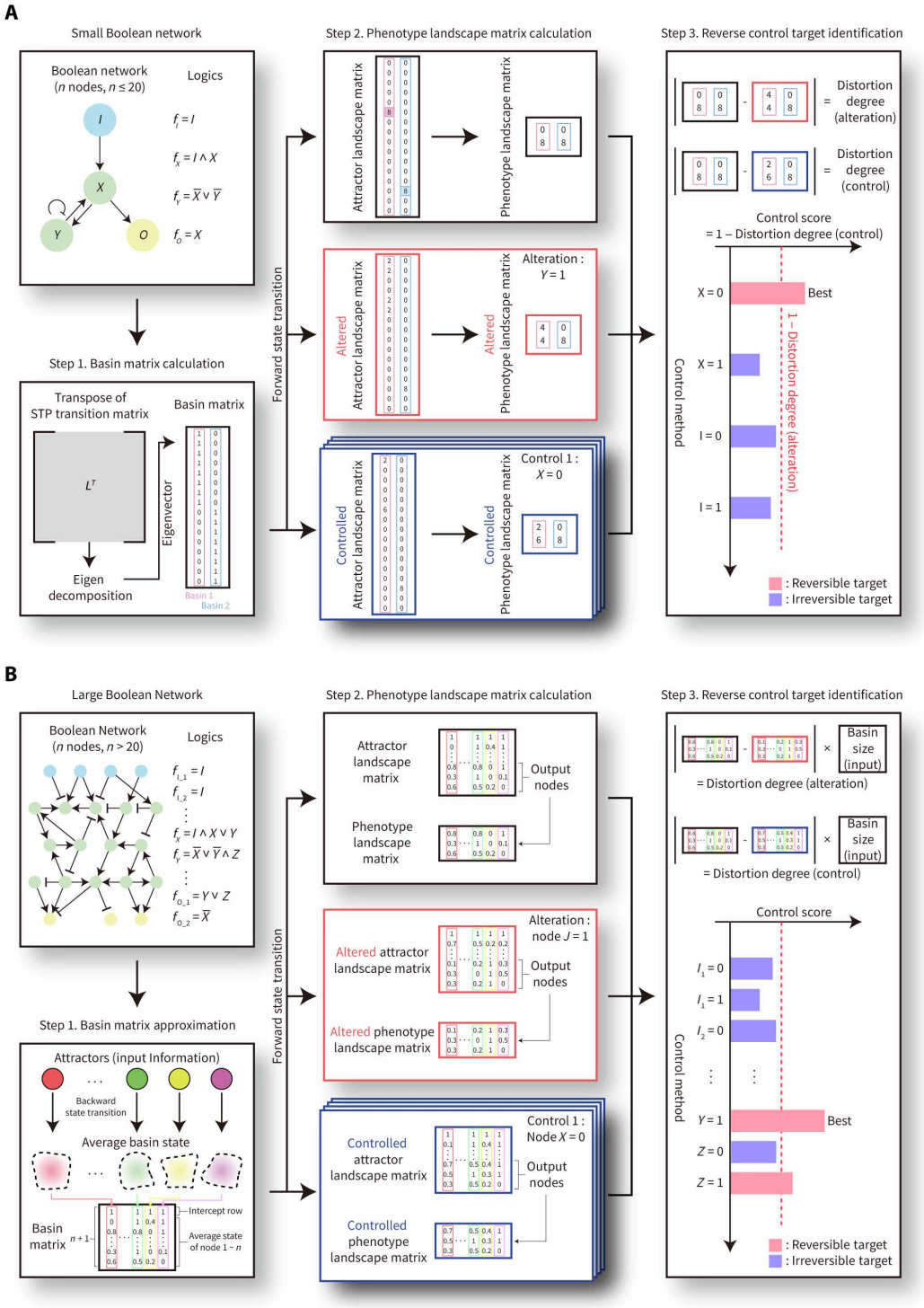

Fig. 2. The ARC framework. (**A**) Exact ARC framework for phenotype landscape reversion of small Boolean networks. The algorithm input is the Boolean network. In step 1, exact basins for each attractor are calculated through eigen decomposition of the transpose of the STP transition matrix. In step 2, reached attractors and corresponding phenotypes for each basin under nominal, altered, and controlled conditions are computed. In step 3, the phenotype landscape matrices under nominal, altered, and controlled conditions are compared to identify the reverse control targets. (**B**) Approximate ARC framework for phenotype landscape reversion of large Boolean networks. The algorithm inputs are the Boolean network, its attractors, and their relative basin size ratios. In step 1, approximated average basins for each attractor are calculated through the backward state transitions. In step 2, reached attractors and corresponding phenotypes for each approximated average basin under nominal, altered, and controlled conditions are computed. In step 3, the phenotype landscape matrices under nominal, altered, and controlled conditions are compared to identify the reverse control targets.

we analyzed 43 Boolean networks from the Cell Collective database and several other previous studies (table S1) (*32*–*36*). We found that the approximate ARC framework empirically achieves 77% accuracy after convergence from consecutive backward and forward state transitions (Fig. 3A and Methods). Theoretically, we proved that the expected upper bound of the approximation error is about 10% for one-step state transition in biological networks (fig. S1 and the Supplementary Materials).

To investigate the approximate ARC framework accuracy for identifying reverse control targets using our algorithm, we analyzed 300 randomly generated Boolean networks. Half of the random networks were sparse, while half were densely connected, where biological networks are known to be generally sparse (*37*–*40*). The details of the random network generation process are explained in Methods. We approximated the rankings of all possible single-node controls and computed the Wasserstein distance between the exact rankings computed by brute force simulation and our rankings to calculate the similarity between them. The approximate ARC framework shows about 90% accuracy in the sparse random networks and 45% accuracy in the dense random networks (Fig. 3B). Because the normality are not guaranteed to the accuracy distributions, we performed the Wilcoxon rank-sum test between two accuracy sets and compute the P value $< 2.2 \times 10^{-16}$. We also computed the average in-degree of various networks including biological networks and observed that the median of the average in-degree of the biological networks is about 2, which is similar to the median of the average in-degree of the sparse random networks (fig. S2) (*39*).

Single-node control targets identified by the ARC framework tend to revert most of the nominal phenotype landscape. We used 33 networks among the 43 biological Boolean networks that contain output nodes, defined as nodes without any child nodes, since the phenotype is defined in terms of the values of output nodes. Using single-node control, 15 of 33 networks can restore at least 90% of the nominal phenotype landscape, and 23 networks can restore at least 80% of the nominal phenotype landscape. Moreover, we observed that the distortion degree of the controlled networks is positively correlated with the distortion degree of the altered network (Fig. 3C). This correlation intuitively suggests that more drastic alterations tend to be less reversible by single-node control.

Last, the effectiveness of phenotype landscape reversion with the ARC framework was compared against two well-established Boolean network control methods. Because no existing method is designed to revert the phenotype landscape as a whole, we focus on the more limited problem of reverting the major attractor. We used the feedback vertex set (FVS) and the logical domain of influence (LDOI)–based global stabilization methods for comparison (*41*, *42*, *12*, *17*). The FVS is defined as a set of nodes whose removal removes all cycles from the network. The LDOI of a given set of nodes and their state values includes those nodes and their corresponding state values that become stabilized after the first logical update of neighboring nodes. We used the same 33 biological networks with output nodes and set the effectiveness of FVS-based method to zero if the major attractor contains oscillating nodes because it is designed for fixed-point attractors. For each network, an altered node and its state values are selected as the node with maximum degree with the opposite state value in the largest attractor to induce a drastic alteration. After the alteration, we compute the phenotype landscape reversion effectiveness for each proposed control target by comparing the phenotype of converged attractors from random initial states under the nominal and controlled conditions through approximated brute force simulations.

We observed that the control targets identified by the ARC framework exhibited the same or higher effectiveness than those identified by other methods, for every network (Fig. 3D). On average, ~85% of the nominal phenotype landscape can be restored through the best single-node control identified by ARC framework, 75% for control identified by the LDOI–based method, and 56% for control identified by the FVS method. After comparing the efficacy of the ARC framework, we also computed the expected required time for target identification in large networks compared to brute force simulation. We observed that the ARC framework is ~77 times faster than the conventional approximated brute force simulation (fig. S3 and Supplementary Text).

Exact reverse control target identification in a small Boolean network

To demonstrate the utility of the exact ARC framework, we investigated a reduced mitogen-activated protein kinase (MAPK) Boolean network to identify potential targets for restoring the phenotype landscape (*43*). The network comprises 4 input nodes, 10 internal nodes, and 3 output nodes (Fig. 4A). In the nominal phenotype landscape, ~76% of the network states represent the apoptosis phenotype, ~15% represent a "no decision" phenotype where cells passively survive with no cell fate decision, and the remaining 9% represent a minor growth arrest phenotype (Fig. 4B). From the perspective of DNA damage, which is one of the input nodes in the MAPK network, all network states with DNA damage turned on eventually converge to the apoptosis phenotype, ensuring the proper removal of damaged cells.

Phosphatase and Tensin homolog deleted on chromosome 10 (PTEN) is a well-known tumor suppressor gene that prevents rapid cell growth and undesired proliferation by antagonizing the phosphatidylinositol 3-kinase (PI3K)–AKT signaling pathway (*44*, *45*). The deletion of PTEN can lead to various cancers, including prostate and bladder cancer (*46*, *47*). The MAPK network reflects the critical distortion in the phenotype landscape under the LoF alteration of PTEN (Fig. 4C). In the altered phenotype landscape, ~99.7% of the network states represent a "no decision" phenotype, while only 0.3% represent the apoptosis phenotype. This distortion indicates that cells with DNA damage are not removed, potentially leading to the initiation of bladder cancer (*43*).

We applied the exact ARC framework to identify reverse control targets for restoring the altered phenotype landscape under the PTEN LoF alteration. The inhibition of PI3K or AKT, both key nodes in the PI3K-AKT signaling pathway, was found to most effectively restore the nominal phenotype landscape (Fig. 4D). Previous studies have shown that AKT inhibitors can induce apoptosis in cells with an activated PI3K-AKT signaling pathway, a result consistent with our analysis (*48*). In the controlled phenotype landscape, ~80% of the network states represent the apoptosis phenotype, about 11% represent a "no decision" phenotype, and the remaining 9% represent a minor growth arrest phenotype.

Furthermore, we analyzed the mechanism of phenotype landscape reversion. Under the PTEN LoF, AKT tends to be fixed as 1 because of the logical function for AKT: AKT = PI3K and not PTEN. When AKT is fixed as 1, the downstream apoptosis and growth arrest nodes are typically fixed as 0, distorting the primary phenotype (Fig. 4E). To revert this distortion, the inhibition of PI3K or AKT reestablishes the PI3K-AKT signaling pathway by consistently maintaining

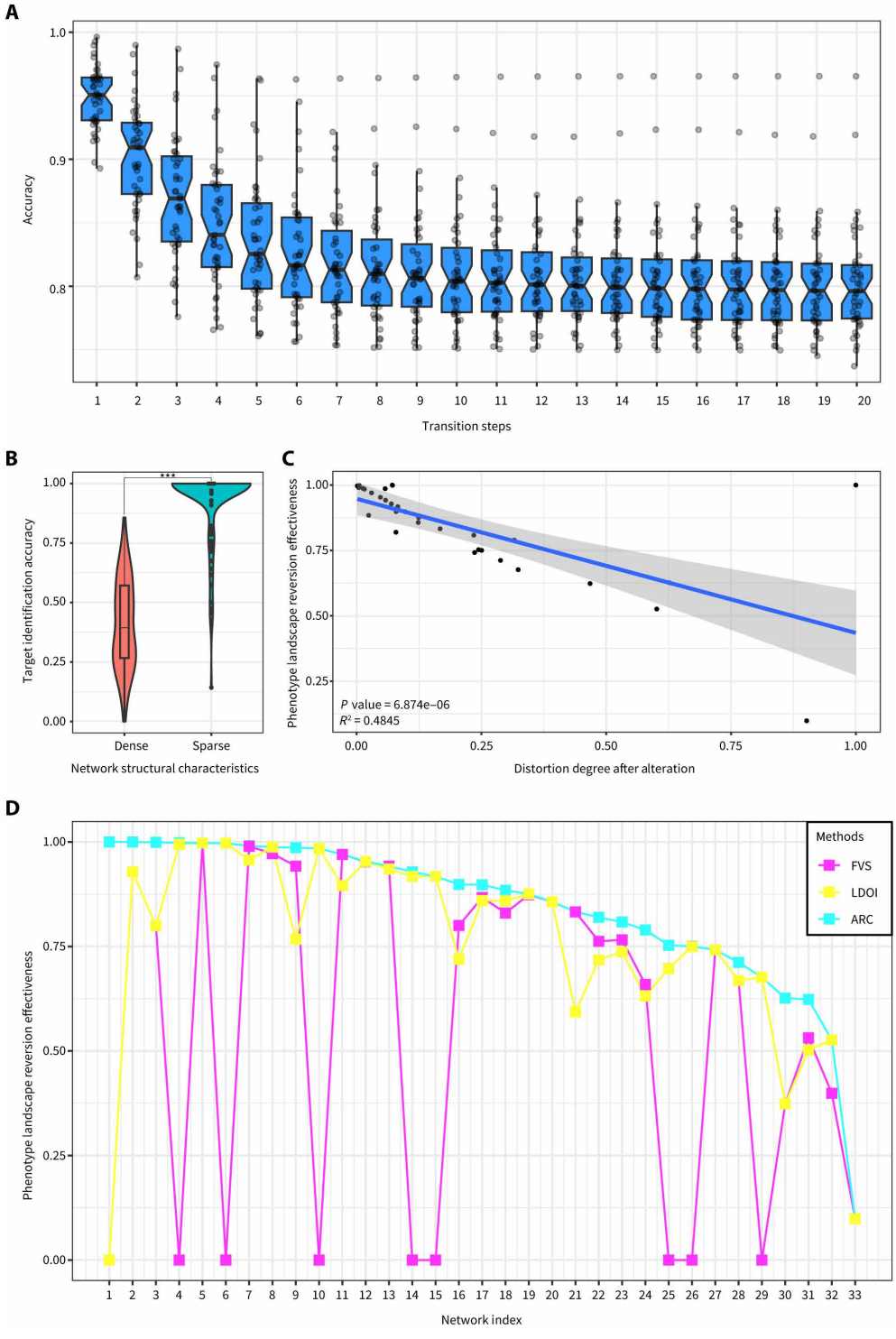

Fig. 3. Phenotype landscape reversion efficacy. (**A**) Converged behavior of the accuracy for the first order Taylor approximation used by the approximated ARC framework. The *x* axis is consecutive backward and forward state transition steps. Each dot represents the accuracy in a single network. (**B**) Comparison of target identification accuracy between sparse networks and dense networks (P value $< 2.2 \times 10^{-16}$). The accuracy in sparse networks is approximately twice that in highly connected networks. (**C**) Linear regression line represents the negative correlation between the distortion degree after alteration and reverse control score of the best single-node control (P value: 6.874×10^{-06}, $R^2 = 0.4845$). Each dot represents the computed value for one of 33 networks. (**D**) Phenotype landscape reversion effectiveness comparison among control methods. Among all 33 biological Boolean networks, control targets identified by the ARC framework are always equally or more effective than other methods. Because the FVS method is only applicable to fixed-point attractors, it has zero phenotype landscape reversion effectiveness on oscillating attractors. LDOI refers to the logical domain of influence.

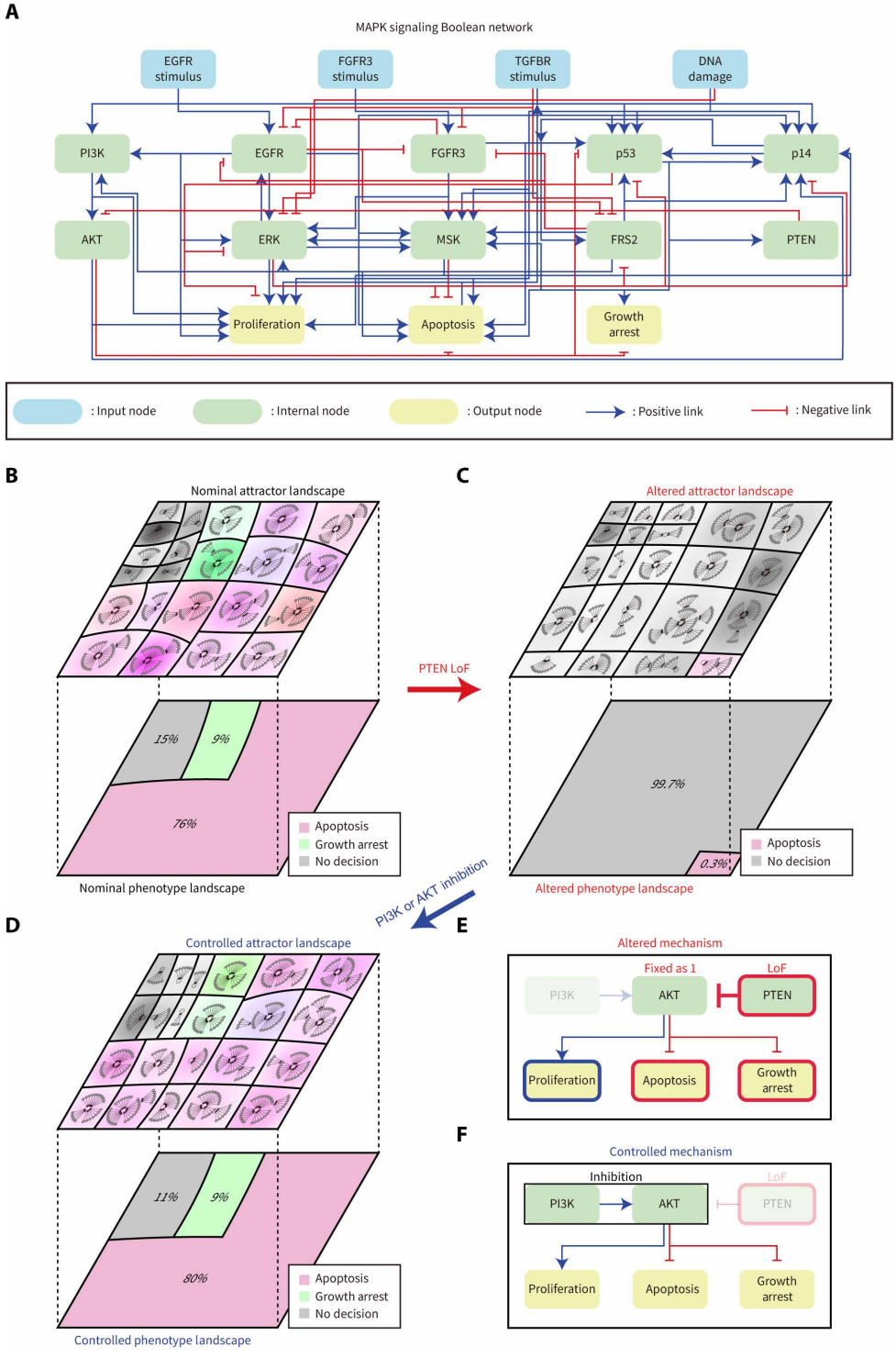

Fig. 4. Reversibility of the MAPK Boolean network. (**A**) MAPK Boolean network. (**B**) Phenotype landscape under nominal conditions. The network exhibits 22 attractors and their corresponding basins in the nominal attractor landscape, each mapped to the nominal phenotype landscape. (**C**) Altered phenotype landscape under a LoF of PTEN. Almost all network states result in a no decision phenotype, which means none of the output nodes are ON. (**D**) Controlled phenotype landscape under inhibition of the PI3K-AKT signaling pathway. This intervention restores the nominal phenotype landscape. (**E**) Mechanism causing the distorted phenotype landscape. The alteration leads to activation of the PI3K-AKT signaling pathway, causing the inhibition of apoptosis and growth arrest nodes, resulting in the no decision phenotype. (**F**) Mechanism restoring the nominal phenotype landscape. Through inhibition of the PI3K-AKT signaling pathway, the flexibility of downstream apoptosis and growth arrest nodes is increased, enabling restoration of the nominal phenotype landscape. EGFR refers to the epidermal growth factor receptor.

these nodes at a value of 0. This restoration increases the flexibility of downstream nodes, such as apoptosis and growth arrest, enabling the regeneration of the original apoptosis phenotype (Fig. 4F).

Approximate reverse control target identification in a large Boolean network

We then applied the approximate ARC framework to the T cell receptor (TCR) signaling Boolean network to identify reverse control targets for restoring the phenotype landscape (*49*). This network consists of 7 input nodes, 79 internal nodes, and 12 output nodes (Fig. 5A). Key inputs—such as CD28, CD4, and TCR signals—drive the activation of transcription factors at output nodes, which are critical for T cell function.

The analysis of the nominal phenotype landscape revealed seven phenotypes from P1 to P7 (Fig. 5B and fig. S4). Four attractors with small basin size ratios were considered negligible, leaving three major phenotypes P1, P2, and P3. P1 has the largest basin size ratio with activated serum response element (SRE), P21c, p277k, and forkhead box protein O1 (FKHR). P2 has the second largest basin size ratio with activated Bcat, Cyc1, BclXL, and p70s, and P3 has the third largest basin size ratio with activated p21c, p27k, and FKHR. Each of them represents a different T cell activation pattern from naïve T cells.

Previous studies have shown that sustained T cell activation without external stimuli can lead to diseases such as leukemia or autoimmunity (*50*, *51*). To simulate this undesired T cell activation, candidate intervention sets inducing sustained full activation of T cells were proposed previously. From these, we introduced a LoF alteration in Gab2 and a GoF alteration in ZAP70. These alterations caused significant changes to the phenotype landscape, particularly due to the activation of AP1, cyclization recombinase (CRE), and nuclear factor of activated T cells (NFAT), which drive sustained T cell activation. The altered phenotype landscape exhibited nine phenotypes, from AP1 to AP9 (Fig. 5C and fig. S4). Phenotypes AP1, AP2, and AP3 were observed in the nominal Boolean network but with altered basin sizes. AP4 and AP8 exhibited activated NFAT, which was absent in the nominal phenotype landscape. AP5, AP6, AP7, and AP9 exhibited simultaneous activation of AP1, CRE, and NFAT, leading to severe distortions in the phenotype landscape. These distortions due to sustained activation of AP1, CRE, and NFAT can cause indiscriminate T cell activation from naïve T cells, which leads to prolonged inflammation and tissue destruction.

Applying the approximate ARC framework, we identified the inhibition of LAT, a downstream node of ZAP70, as the most effective control target for restoring the nominal phenotype landscape (*52*). This inhibition successfully restored the phenotype landscape to its nominal state, resulting in three phenotypes, from CP1 to CP3 (Fig. 5D and fig. S4). Specifically, the three major phenotypes (P1, P2, and P3) were preserved, corresponding directly to the restored phenotypes (CP1, CP2, and CP3). Basins and phenotype distributions were also similar to the nominal phenotype landscape, with negligible phenotypes excluded due to their small basin size ratios.

Under nominal conditions, the expression of AP1 and CRE is regulated by the c-Jun N-terminal kinase (JNK)/Jun and Ras/MAPK kinase (MEK)/extracellular signal–regulated kinase (ERK) pathways (*53*, *54*). These pathways are influenced by upstream nodes, with VAV1 and sh3bp2 controlling the JNK/Jun pathway and Gads, PLCgb, and SLP76 controlling the Ras/MEK/ERK pathway. However, the combined Gab2 LoF and ZAP70 GoF alterations fix LAT and SLP76 to 1, disrupting the regulation of both pathways and resulting in dysregulated AP1 and CRE expression patterns (Fig. 5E). To restore the phenotype landscape, the suppression of LAT releases this fixation, reestablishing normal regulation of VAV1, sh3bp2, Gads, and PLCgb (Fig. 5F). Consequently, the expression patterns of AP1 and CRE return to their nominal states, enabling the restoration of the phenotype landscape.

DISCUSSION

Distortions in the nominal dynamic behavior of biological systems caused by various alterations present significant challenges for their survival. Current methods for controlling biological Boolean networks primarily focus on determining the fate of systems or cells by fixing certain network nodes to achieve a single desired outcome, such as driving all cancer cell states to a single normal or normal-like states through targeted molecular interventions. However, these approaches fall short of restoring nominal dynamic behavior that reestablishes proper response patterns under diverse conditions. In this study, we introduced the ARC framework to reverse distorted phenotype landscapes, which represent the dynamic behavior of biological systems. The ARC framework can achieve the restoration of nominal dynamic behavior under altered conditions by identifying control targets, which can reverse the distortions.

The ARC framework can quantitatively measure the distortion degree of phenotype landscapes in altered biological networks and identify potential reverse control targets algebraically, unlike existing methods that focus on achieving a single desired state or disregard which basins lead to which phenotypes. Phenotype landscapes provide essential insights on how biological networks can produce varying responses to the same input stimulus due to differences in their internal environments. States within each basin can represent enriched biological pathways or activated motifs in the Boolean network, which cannot be identified based solely on input node values. Hence, restoring nominal behavior requires analyzing the entire basin within the phenotype landscape, which encompasses both input and internal node values.

To enable this analysis, we developed a method to identify the entire basin through eigen decomposition of the transpose of the STP transition matrix. By consecutively multiplying the STP transition matrix with the basin, we can analyze the phenotype landscape algebraically. Quantifying phenotype landscape distortion and reversion effects allows the ARC framework to provide a detailed analysis and higher sensitivity in identifying effective reverse control targets for reversion of the phenotype landscape.

While the STP-based methodology enables precise quantification of phenotype landscapes, it becomes computationally impossible for large Boolean networks due to its exponential complexity. To address this limitation, we extended our approach using a first-order Taylor approximation of the polynomial forms of Boolean functions. This approximation reduces computational complexity while preserving the linearity needed to analyze the backward STG with high accuracy, allowing us to apply the method to large networks. Furthermore, the ARC framework is more effective at phenotype landscape reversion compared to several well-established Boolean network control strategies and ensures the accurate identification of reverse control targets in sparse networks. Consequently, the ARC framework provides an algebraic strategy for analyzing phenotype landscapes, including those of large biological Boolean networks.

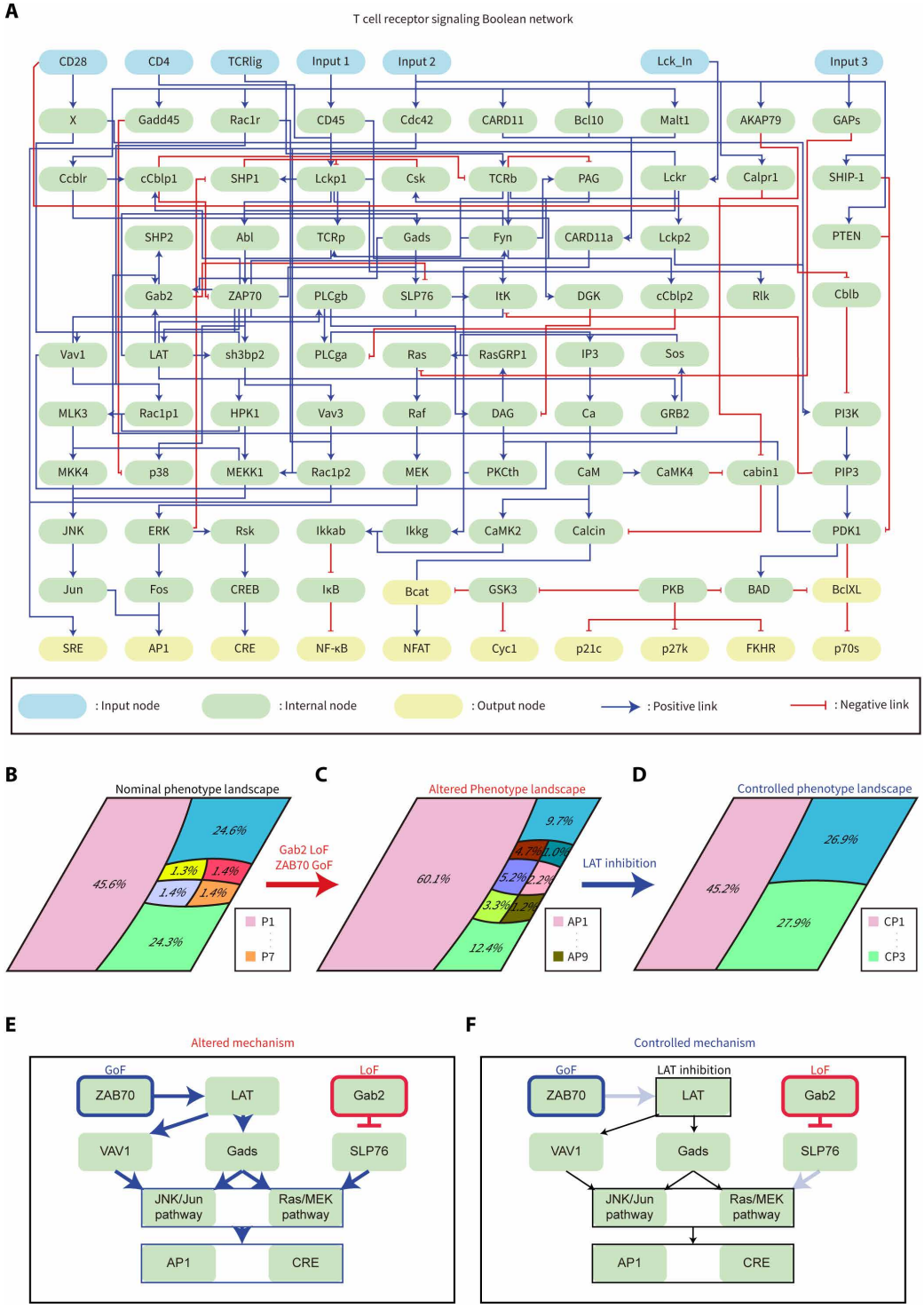

Fig. 5. Reversibility of the TCR signaling Boolean network. (**A**) TCR signaling Boolean network. (**B**) Phenotype landscape under nominal conditions. Half of the states produce the P1 phenotype, half of the remaining states produce the P2 phenotype, and the rest primarily produce the P3 phenotype. Other phenotypes have relatively small basin sizes. (**C**) Altered phenotype landscape under LoF of Gab2 and GoF of ZAP70. States from the basins of P2 and P3 now produce the AP1 phenotype, which is equivalent to P1. Other phenotypes are also distorted. (**D**) Controlled phenotype landscape under suppression of LAT. The three major phenotypes from the nominal phenotype landscape, P1, P2, and P3, are restored as CP1, CP2, and CP3. (**E**) Mechanism causing the distorted phenotype landscape. Because of the alterations, the JNK/Jun pathway and Ras/MEK/ERK pathway are dysregulated, leading to abnormal activation of AP1 and CRE. (**F**) Mechanism restoring the nominal phenotype landscape. Through suppression of LAT, the JNK/Jun pathway and Ras/MEK/ERK pathway are properly regulated, restoring normal phenotype landscape dynamics. NF-κB, nuclear factor κB; IκB, inhibitor of nuclear factor B.

The identification of reverse control targets for phenotype landscape reversion suggests different insights into control strategies for biological systems. Conventional control methods typically reduce system entropy by fixing node values, limiting the ability of the system to respond dynamically under nominal conditions. In contrast, reversing phenotype landscapes necessitates reintroducing eliminated responses, which requires increasing system entropy. In many biological contexts, such as information-processing in cell signaling, functional flexibility is essential to generate different responses depending on the external stimulus. This functional diversity can be viewed as the entropy of the network. Remarkably, we observed that the entropy of the network often increases following the intervention of reversible control targets found by our algorithm. Therefore, the ARC framework may be especially beneficial in biological contexts that require functional flexibility to recover behavior similar to that of the nominal system.

Reverting phenotype landscapes is inherently more complex than producing a single desired system response. Achieving this goal requires restoring the ability of altered biological systems to generate appropriate responses across multiple internal and external conditions. Our approach provides an algebraic framework for quantifying reversion effects and identifying control targets, offering a valuable tool for addressing this challenge. As a current limitation, cyclic attractors are handled by averaging their states, which may oversimplify their dynamics. This simplification could affect the accuracy of phenotype landscape reversion in networks with prominent cyclic behaviors. Future work could enhance the accuracy of this method by exploring higher-order approximations or suggesting other strategies to deal with the cyclic attractors. In addition, the experimental validation of identified control targets will be crucial for translating these findings into practical applications in systems biology and therapeutic development.

METHODS

Boolean network models

To systematically analyze the dynamic behavior of biological systems, we use mathematical models that represent system dynamics. In particular, we use the Boolean network model, one of the simplest mathematical models, which effectively captures the essential dynamics of biological systems. In a Boolean network, each node represents a molecular component, such as a gene or protein, and is assigned a binary state either 1 (active) or 0 (inactive). The edges represent regulatory interactions between nodes, with a direction indicating influence from an upstream node to a downstream node. The effect on the downstream node is formalized by a Boolean function f_i for the i-th node, which integrates the regulatory effects of its upstream nodes. The state of a Boolean network is defined as the collection of all node states at a given time. The network state vector $\mathbf{x}(t)$ at specific time t can be expressed as

$$\mathbf{x}(t) = \{x_1(t), \cdots, x_i(t), \cdots, x_N(t)\}$$

where N is the total number of nodes in the network, and $x_i(t)$ is the state of i-th node at time t. The state of the i-th node at the next time step is determined by the Boolean function $f_i\left(x_{j\in I_i}\right)$, where I_i is the set of upstream nodes indices for the i-th node. This relationship can be expressed as

$$x_i(t+1) = f_i\{x(t)_{j\in I_i}\}$$

Consequently, the network state vector at the next time step is given by the following synchronous update scheme

$$\mathbf{x}(t+1) = \left[f_1\{x(t)_{j\in I_1}\}, \cdots, f_i\{x(t)_{j\in I_i}\}, \cdots, f_N\{x(t)_{j\in I_N}\}\right]$$

When the i-th node is altered, its Boolean function is also modified. In a LoF alteration, the Boolean function is altered to $f_i\{x(t)_{j\in I_i}\} = 0$, meaning the node becomes permanently inactive. In a GoF alteration, the Boolean function is altered to $f_i\{x(t)_{j\in I_i}\} = 1$, meaning the node becomes permanently active.

Algebraic representation of state transitions in Boolean networks through STP

Using the STP, which generalizes matrix products for matrices of any dimensions, the logical expressions in the Boolean update scheme can be converted into a linear matrix product form (*24*). This representation converts a Boolean network model into a linear system (*25*). The STP operation, denoted by $\ltimes$, is defined as

$$X \ltimes Y = \sum_{i=1}^{p} X^i y_i$$

where X is a row vector of dimension np, Y is a column vector of dimension p; X^i represents the i-th subvector of X, divided equally into p subvectors; and y_i represents the i-th element of Y. For example, X^2 represents the second subvector of X, which is composed of the elements of X from indices n to $2n$. To convert a Boolean network model into a linear system, the network state vector $\mathbf{x}(t)$ must be converted into STP-based network state vector $s(t)$ of dimension 2^N. The vector $\mathbf{s}(t)$ is computed as

$$\mathbf{s}(t) = \{\ltimes_{i=1}^{N} c_i(t)\}$$

where $c_i(t) = \begin{bmatrix} 1 \\ 0 \end{bmatrix}$ if $x_i(t) = 1$, and $c_i(t) = \begin{bmatrix} 0 \\ 1 \end{bmatrix}$ if $x_i(t) = 0$. Thus, every 2^N network state vector $\mathbf{x}(t)$ has a one-to-one correspondence to $\delta_{2^N}^i$ in descending order, where $1 \le i \le 2^N$ and $\delta_{2^N}^i$ represents the i-th column vector of $2^N \times 2^N$ identity matrix. Then, we defined the transfer function T and its inverse T^{-1} as

$$T\{\mathbf{x}(t)\} = \mathbf{s}(t), T^{-1}\{\mathbf{s}(t)\} = \mathbf{x}(t)$$

After converting $\mathbf{x}(t)$ into $\mathbf{s}(t)$, $\mathbf{s}(t+1)$ is computed through linear multiplication with the $2^N \times 2^N$ STP transition matrix L

$$\mathbf{s}(t+1) = L \times \mathbf{s}(t)$$

The i-th column of L represents the next time step of the STP-based network state vector of $\mathbf{s}(t)$ which corresponds to $\delta_{2^N}^i$ (Fig. 6, A and B). Thus, the column vectors of L and their column indices represent all transitions in the forward STG of the given Boolean network. Consequently, the state transition of the Boolean network is reformulated as a matrix product between L and $\mathbf{s}(t)$. We further prove that eigenvectors of L corresponding to an eigenvalue of 1 represent attractor vectors in the STP format (Fig. 6C and the Supplementary Materials).

To fully analyze the phenotype landscape, both phenotypes and their corresponding basins must be identified. To identify basins, we use the concept of backward state transitions in Boolean networks through time reversal (Fig. 6D). By reversing the directions of the arrows in the STG, a backward STG can be constructed (Fig. 6E).

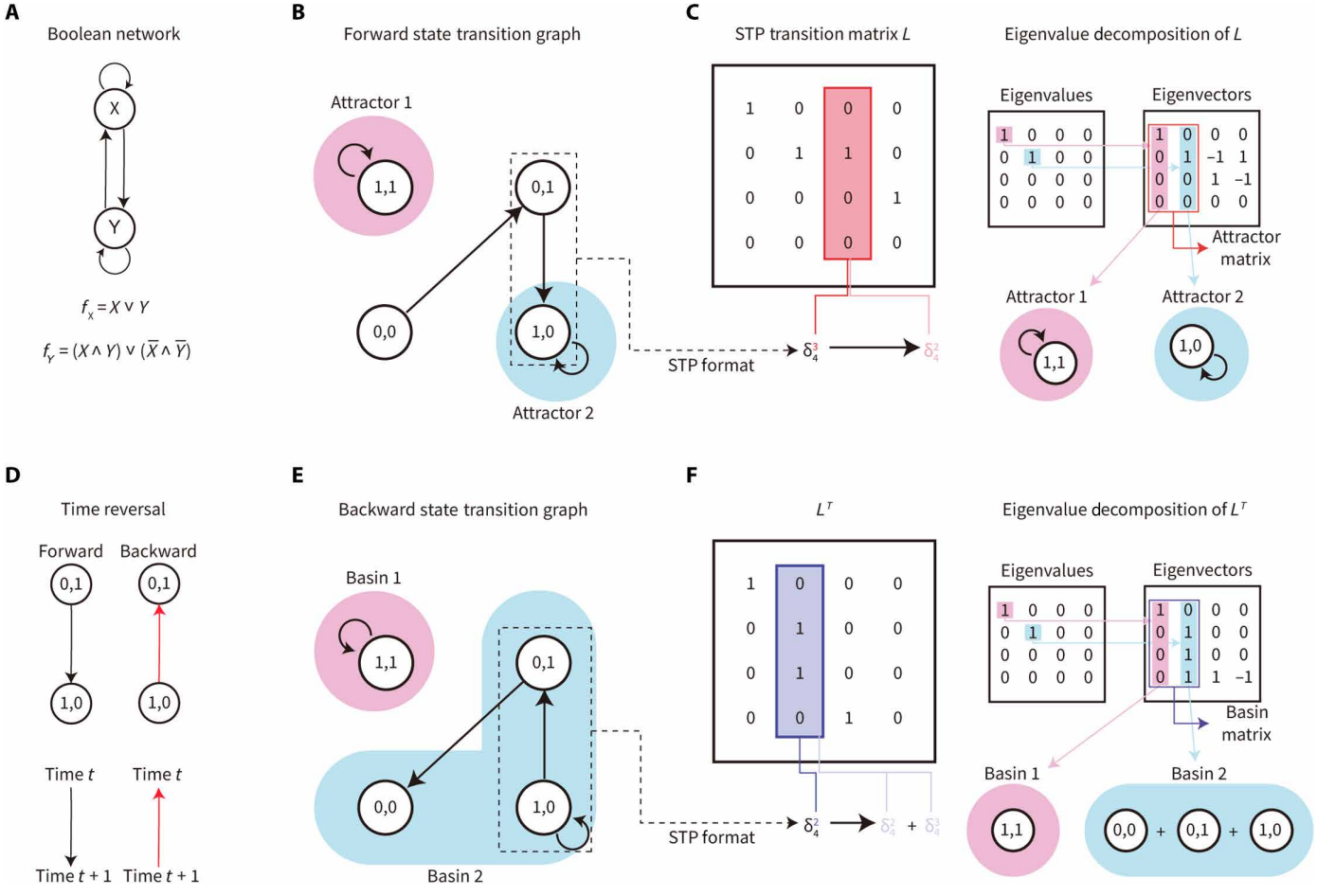

Fig. 6. Identification of attractors and basins. (**A**) Toy Boolean network with two nodes and their corresponding Boolean update functions. (**B**) Forward STG of the toy Boolean network. Each arrow represents a state transition, and states with colored backgrounds represent attractors. (**C**) Corresponding state transition matrix *L*. In the STG, the pretransition state determines the column index of *L*, while the posttransition state determines the column elements. Eigenvectors with an eigenvalue of 1 correspond to each attractor. (**D**) Backward state transition process in the time-reversal Boolean network. (**E**) Backward STG of the toy Boolean network. Each arrow represents a backward state transition, and colored backgrounds represent basins. (**F**) Transpose of *L*, corresponding to the backward state transition matrix. Eigenvectors with an eigenvalue of 1 correspond to each basin.

Note that past states map to future states in a many-to-one manner due to synchronous update, such that many past states converge to the same attractor. Despite this asymmetry in time, we prove that the backward STP transition matrix is equivalent to L^T (Fig. 6F and the Supplementary Materials). The backward state transition can be converted into linear multiplication as

$$\sum s(t-1) = L^T \times s(t)$$

where $\sum s(t-1)$ is sum of the past states, which become $s(t)$ in the next time step. Furthermore, we demonstrate that eigenvectors of L^T corresponding to an eigenvalue of 1 represent basin vectors in the STP format (see the Supplementary Materials).

Matrix representation of the phenotype landscape in the exact framework

To represent the phenotype landscape of Boolean network algebraically, we first compute the attractors reached by each basin in the nominal attractor landscape. This can be calculated as $L^k \times B$, where k is the diameter of the STG and B is the basin matrix of the Boolean network. The basin matrix is a $2^n \times m$ matrix, where m is the number of basins in the nominal Boolean network. Each row of the basin matrix represents all possible network state vectors in the Boolean network with n nodes indexed in descending binary order. If $B_{i,j}$ is 1, meaning the (i,j)-th element of the basin matrix is 1, then the i-th network state belongs to the j-th basin. Whereas if $B_{i,j}$ is 0, then the i-th network state does not belong to the j-th basin. The basin matrix can be computed through the eigen decomposition of L^T, where the eigenvectors of L^T corresponding to an eigenvalue of 1 constitute the column vectors of B. After we calculate $L^k \times B$, we can get an attractor landscape matrix of size $2^n \times m$ matrix, where (i,j)-th element of the attractor landscape matrix is 1 if i-th network state is an attractor of j-th basin and 0 otherwise.

The phenotype of each attractor is defined as the collection of output node states in that attractor. To compute this algebraically from the attractor landscape matrix, we generate an attractor-to-phenotype converter (APC) matrix, which is a $2^{|O|} \times 2^N$ matrix. Here, $|O|$ represents the number of output nodes, and $2^{|O|}$ represents the

number of distinct phenotypes. The i-th column of the APC matrix is computed as

$$\mathrm{APC}_i = T^{-1}\left(\delta^i_{2^N}\right)[O]$$

where $[O]$ extracts the indices corresponding to the output nodes. Using this, the phenotype landscape matrix under the nominal condition (PLM_N) of size $2^{|O|} \times m$ is computed as

$$\mathrm{PLM}_N = \mathrm{APC} \times L^k \times B$$

Each column index of PLM_N corresponds to a basin in the nominal phenotype landscape, and the column vector represents the distribution of phenotypes in the attractor reached by that basin. Under the nominal condition, each basin must represent one phenotype. However, under the altered or controlled conditions, a distribution of phenotype can arise because a one-to-one mapping between phenotypes of the nominal basins and those under the altered or controlled conditions cannot be guaranteed.

Alteration effect on the phenotype landscape in the exact framework

To model the effects of alterations (or controls) on the state transition process, we develop an effect matrix (E). The alteration effect is encoded in the matrix E, incorporating the effect on state vectors through matrix multiplication, expressed as

$$\text{Altered } \mathbf{s}(t) = E \times \mathbf{s}(t)$$

The i-th column vector of E for the single-node alteration is computed as

$$E_i = \begin{cases} \delta^i_{2^N} \text{ if } STP^{-1}\left(\delta^i_{2^N}\right)[A] = \sigma(A) \\ \delta^j_{2^N} \text{ if } STP^{-1}\left(\delta^i_{2^N}\right)[A] \neq \sigma(A) \end{cases}$$

where $[A]$ represents the index of altered node, $\sigma(A)$ denotes the altered node value, and $\sigma^j_{2^N}$ corresponds to the STP-based network state of altered $\boldsymbol{x}(t)$. If no alteration occurs, then E is equivalent to the $2^N \times 2^N$ identity matrix. To compute the E for the multiple node alteration, it can be obtained by multiplying the E of the individual single-node alterations that together constitute the multiple node alteration regardless of the multiplication order.

Using this framework, we compute the PLM under alteration condition, denoted as PLM_A, as

$$\mathrm{PLM}_A = \mathrm{APC} \times (E \times L \times E)^k \times B = \mathrm{APC} \times E \times (L \times E)^k \times B$$

The second equality holds since E is an idempotent matrix.

We quantify the degree of distortion in the phenotype landscape due to alterations using the following formula

$$\text{Distortion Degree} = \frac{1}{2^N}\left\|\mathrm{PLM}_N - \mathrm{PLM}_A\right\|_{1,1}$$

where $\|A\|_{1,1} = \sum_{i=1}^{m}\sum_{j=1}^{n}|a_{ij}|$ for $m \times n$ matrix A. The normalization ensures that the distortion degree is expressed as a numerical value between 0 and 1, where 0 indicates no distortion and 1 indicates complete distortion.

To identify reverse control targets, first we define the control score as

$$\text{Control Score} = 1 - \text{Distortion Degree}$$

To compute the control score for the control, we calculate the distortion degree between PLM_N and controlled phenotype landscape matrix (PLM_C). Control targets, similar to alterations, set a node to a fixed value. PLM_C is then computed as

$$\mathrm{PLM}_C = \mathrm{APC} \times C \times (L \times C)^k \times B$$

where C is an effect matrix for both control when the altered nodes are fixed to altered states and controlled nodes are fixed to controlled states together. We define a reverse control target as a target node state that produces a smaller distortion degree between PLM_N and PLM_C, in other words, produces a largest control score.

Taylor approximation of STP in the approximate framework

We extend our methodology to an approximate ARC framework for analyzing and identifying reverse control targets for phenotype landscape reversion in large Boolean networks, defined as networks containing more than 20 nodes. The computational complexity of STP-based methods prohibits their direct application to large networks. Brute force simulations could be used to analyze the phenotype landscape, but still this approach is limited as it can only identify major attractors and their relative basin size ratios rather than complete basin states. This lack of basin information obstructs the comprehensive analysis of phenotype landscapes.

To overcome these limitations, we approximate the forward and backward state transition matrices, L and L^T, by generating normalized coefficient matrices derived from the first-order Taylor approximation of the polynomial representation of each Boolean update function f_i. For each f_i, the polynomial representation p_i is computed as

$$p_i = \sum_{n_1=0}^{1}\sum_{n_2=0}^{1}\cdots\sum_{n_{|I_i|}=0}^{1}\left\{f_i\left(n_1, n_2, \cdots n_{|I_i|}\right) \times \prod_{x_j \in I_i}\left(x_j^{n_j} \times \left(1 - x_j\right)^{1-n_j}\right)\right\}$$

where n_j represents the j-th node state among upstream regulator nodes of i-th node and I_i is the set of upstream nodes for the i-th node. After converting the Boolean update logic f_i into its polynomial representation p_i, we apply a first-order Taylor approximation to obtain linear equations between i-th node and its upstream regulator nodes. For a node with $|I_i|$ upstream regulators, we approximate p_i at all $2^{|I_i|}$ possible points, from $(0, 0, \cdots, 0)$ to $(1, 1, \cdots, 1)$, and average the equations to derive the linear approximation. This average approximation is computed as

$$p_i \approx \frac{1}{2^{|I_i|}}\sum_{n_1=0}^{1}\sum_{n_2=0}^{1}\cdots\sum_{n_{|I_i|}=0}^{1}\left[f_i\left(n_1, n_2, \cdots n_{|I_i|}\right) + \sum_{x_j \in I_i}\left\{\frac{\partial p_i\left(n_1, n_2, \cdots n_{|I_i|}\right)}{\partial x_j} \times \left(x_j - n_j\right)\right\}\right]$$

subject to $p_i^{\min} \leq p_i \leq p_i^{\max}$, where $p_i^{\min}$ and $p_i^{\max}$ are the minimal and maximal approximated function values over all possible states of the parents of the i-th node. Since p_i represents node states in the Boolean network, its range is limited to [0,1]. Therefore, to standardize p_i, we normalize it as

$$\text{normalized } p_i = \frac{p_i}{p_i^{\max} - p_i^{\min}} - \frac{p_i^{\min}}{p_i^{\max} - p_i^{\min}}$$

Using the normalized p_i for each node, we construct the approximated forward transition matrix L'_F, which has a size of $(N+1)\times(N+1)$, with the first row and column corresponding to intercept term in the Taylor approximation. Each element of L'_F is computed as

$$L'_F(i,j)=\begin{cases}1 & \text{if } i=1 \text{ and } j=1\\ 0 & \text{if } i=1 \text{ and } j>1\\ \text{normalized } p_{i-1}(0,0,\cdots,0) & \text{if } i>1 \text{ and } j=1\\ \dfrac{\partial(\text{normalized } p_{i-1})}{\partial x_{j-1}} & \text{if } i>1 \text{ and } j>1\end{cases}$$

To approximate L^T, we need to construct a backward node update truth table for each node. Let D_i represent the downstream nodes regulated by the i-th node and U_i represent the union of the upstream regulator nodes of every node in D_i. We can construct truth table with $2^{|U_i|}$ rows and $(|U_i|+|D_i|)$ columns. In this table, the input values correspond to the node states in U_i, while the output values correspond to the node states in D_i, as the nodes in U_i regulate the nodes in D_i. After constructing this extended truth table, we can inversely determine the node states in U_i based on the node states in D_i. Specifically, the i-th node state can be determined using the states of nodes in D_i. For a given set of node states in D_i, $n_{i_1}, n_{i_2}, \cdots, n_{i_{|D_i|}}$, let g_i be a function that determines the i-th node state based on the node states in D_i. If there exists a row where $x_{i_1}=n_{i_1}, \cdots, x_{i_{|D_i|}}=n_{i_{|D_i|}}$, then the function g_i is computed as

$$g_i\left(n_{i_1},\cdots,n_{i_{|D_i|}}\right)=\frac{\#\text{ of rows where } x_{i_1}=n_{i_1},\cdots,x_{i_{|D_i|}}=n_{i_{|D_i|}},x_i=1}{\#\text{ of rows where } x_{i_1}=n_{i_1},\cdots,x_{i_{|D_i|}}=n_{i_{|D_i|}}}$$

Otherwise, if there is no row where $x_{i_1}=n_{i_1}, \cdots, x_{i_{|D_i|}}=n_{i_{|D_i|}}$, then $g_i=0$. Let q_i be polynomial representation of g_i. Then, q_i can be computed as

$$q_i=\sum_{n_{i_1}=0}^{1}\sum_{n_{i_2}=0}^{1}\cdots\sum_{n_{i_{|D_i|}}=0}^{1}\left\{g_i\left(n_{i_1},n_{i_2},\cdots,n_{i_{|D_i|}}\right)\times\prod_{x_j\in D_i}\left(x_j^{n_{ij}}\times(1-x_j)^{1-n_{ij}}\right)\right\}$$

After converting g_i into q_i, it can be approximated linearly and normalized as

$$q_i\approx\frac{1}{2^{|D_i|}}\sum_{n_{i_1}=0}^{1}\sum_{n_{i_2}=0}^{1}\cdots\sum_{n_{i_{|D_i|}}=0}^{1}\left[g_i\left(n_{i_1},n_{i_2},\cdots,n_{i_{|D_i|}}\right)+\sum_{x_j\in D_i}\left\{\frac{\partial q_i\left(n_{i_1},n_{i_2},\cdots,n_{i_{|D_i|}}\right)}{\partial x_j}\times\left(x_j-n_{i_j}\right)\right\}\right]$$

$$\text{normalized } q_i=\frac{q_i}{q_i^{\max}-q_i^{\min}}-\frac{q_i^{\min}}{q_i^{\max}-q_i^{\min}}$$

Using the normalized q_i, we construct the approximated backward transition matrix L'_B, which has a size of $(N+1)\times(N+1)$. Each element of L'_B is computed as

$$L'_B(i,j)=\begin{cases}1 & \text{if } i=1 \text{ and } j=1\\ 0 & \text{if } i=1 \text{ and } j>1\\ \text{normalized } q_{i-1}(0,0,\cdots,0) & \text{if } i>1 \text{ and } j=1\\ \dfrac{\partial(\text{normalized } q_{i-1})}{\partial x_{j-1}} & \text{if } i>1 \text{ and } j>1\end{cases}$$

Matrix representation of the phenotype landscape in the approximate framework

To algebraically represent the phenotype landscape of a large Boolean network, we need to compute the basin matrix B' in large networks. In the approximate ARC framework, the basin matrix is a $(n+1)\times m$ matrix, where the n is the number of nodes and m is the number of major basins considered. The first row consists entirely of ones, which represent the intercept term of first-order Taylor approximation. The remaining n rows contain the average state values of the n nodes for each basin. For a given basin b, the average node state values are defined as $\frac{1}{|b|}\sum_{x_j\in b}x_j$, where $x_j\in b$ denotes a network state included in basin b and $|b|$ is the number of these states in the basin. Because it is impossible to know about the all network states that constitute each basin in a large network, we approximate the B' as

$$B'=L'^{k}_B\times A'$$

where k is a parameter with a default value of 15, A' is the attractor matrix of the large Boolean network, and L'_B is an approximated backward state transition matrix. Here, the A' is also $(n+1)\times m$ matrix where the first row entirely consists of ones and remaining n rows, the remaining n rows represent the considered major attractor state identified through the simulation, and the m is the number of considered major attractors. If the major attractor is a cyclic attractor, then we use the average state value of the cyclic attractor as the major attractor state value.

After computing B', we approximate the attractors reached by each basin in the nominal attractor landscape, similarly to the exact ARC framework. This can be expressed as

$$L'^{k}_F\times B'$$

To compute the phenotype landscape matrix in the approximate ARC framework, we construct an approximated APC (APC′) matrix. The APC′ matrix has dimensions $|O|\times(1+N)$, where $|O|$ is the number of output nodes and N is the total number of nodes in the network. Each column of APC′ is defined, such that the i-th column is a vector of 1 if the $(i-1)$-th node is an output node and 0 otherwise. Using APC′ for the approximate ARC framework, the phenotype landscape matrix under nominal condition (PLM_N') has a size of $|O|\times m$ and is computed as

$$\text{PLM}'_N=\text{APC}'\times L'^{k}_F\times B'$$

Each column index of PLM_N' corresponds to a basin index in the nominal phenotype landscape. The respective column vector represents the output node states in the attractor reached by that basin.

Alteration effect on the phenotype landscape in the approximate framework

To introduce and model the effects of alterations (or controls) on the state transition process in the approximate ARC framework, we

develop an approximated effect matrix (E'). The i-th column vector of E' for the single-node alteration is computed as

$$E_i' = \begin{cases} \delta^1_{N+1} & \text{if } i = 1 \\ 0 & \text{if } i > 1 \text{ and } \exists \text{ LoF of } x_{i-1} \\ \delta^1_{N+1} & \text{if } i > 1 \text{ and } \exists \text{ GoF of } x_{i-1} \\ \delta^1_{N+1} & \text{otherwise} \end{cases}$$

If no alteration occurs, then E' is equivalent to the $(N+1) \times (N+1)$ identity matrix. To compute E' for a multiple node alteration, E' from the corresponding individual single-node alterations can be multiplied together (in any order), as in the exact ARC framework. Using this framework, we compute the PLM under the alteration condition, denoted as PLM'_A as

$$\mathrm{PLM}'_A = \mathrm{APC}' \times \left(E' \times L'_F \times E'\right)^k \times B' = \mathrm{APC}' \times E' \times \left(L'_F \times E'\right)^k \times B'$$

Furthermore, to quantify the distortion degree in the phenotype landscape approximate ARC framework, we consider basin size ratios and defined the distortion degree as

$$\text{Distortion Degree} = \frac{1}{N \times |\text{Attractors}|} \left\| \left(\mathrm{PLM}'_N - \mathrm{PLM}'_A\right) \times D_{\mathrm{R}} \right\|_{1,1}$$

where $|\,\text{Attractors}\,|$ is the number of attractors considered and D_{R} is a diagonal matrix whose diagonal elements correspond to the basin size ratios. We can get the basin size ratios from the initial simulation to identify the considered major attractors.

To identify reverse control targets, we calculate the distortion degree between $\mathrm{PLM}'_N$and the controlled phenotype landscape matrix (PLM'_C). PLM'_C is computed as

$$\mathrm{PLM}'_C = \mathrm{APC}' \times C' \times \left(L'_F \times C'\right)^k \times B'$$

where C' is an effect matrix for control. Then, we define a reverse control target for phenotype landscape reversion in the approximate ARC framework as a target with smaller distortion degree between PLM'_N and PLM'_C than the distortion degree between PLM'_N and PLM'_A. In other words, we identify the best reverse control target, which has a largest control score defined as

$$\text{Control Score} = 1 - \text{Distortion Degree}$$

Accuracy of attractor retention rate in the approximate framework

We calculate the accuracy of the approximated backward and forward state transition processes by comparing them to simulation results. We start from the attractor vectors and compare it with the approximated attractor vectors through backward and forward state transition processes. The error is computed as

$$\text{error} = \frac{1}{20} \sum_{k=1}^{20} \sum_{A_i \in A} \frac{|\,A_i\,| \times \left\| A_i - L'^{\,k}_F \times L'^{\,k}_B \times A_i \right\|_1}{N}$$

where A represents the set of major attractors, $A_i \in A$ denotes each major attractor in the set and $|\,A_i\,|$ is the basin size ratio of the i-th major attractor. Then, the accuracy is computed as

$$\text{accuracy} = 1 - \text{error}$$

Entropy of Boolean networks

We define entropy as the Shannon entropy of each node, where the probability represents the likelihood of the node state being in 1. The Shannon entropy of a node, with the probability p lying between 0 and 1, is computed as

$$\text{Shannon Entropy} = -p\log_2 p - (1-p)\log_2(1-p)$$

where p represents the probability of the node state being in 1. If $p = 0$ or $p = 1$, then the entropy is 0. The entropy of a Boolean network is then defined as the average Shannon entropy of all network nodes, excluding mutated or controlled nodes.

Random Boolean networks generation

We generate 300 random Boolean networks with an equal number of 6-node, 8-node, and 10-node networks. Half of the networks are sparse, with an average in-degree of either 1 or 2. The other half of the networks are dense, with an in-degree of $n-1$ or n, given a network with n nodes. The relationship between sparse networks and real biological networks is explained in the Supplementary materials (Supplementary Text and fig. S2). The code to randomly generate these Boolean networks are provided in our GitHub repository.

Supplementary Materials

This PDF file includes:

Supplementary Text
Figs. S1 to S4
Table S1
References

REFERENCES AND NOTES

1. M. B. Sporn, A. B. Roberts, Autocrine growth factors and cancer. *Nature* **313**, 745–747 (1985).
2. M. A. O'Brien, R. Kirby, Apoptosis: A review of pro-apoptotic and anti-apoptotic pathways and dysregulation in disease. *J. Vet. Emerg. Crit. Care* **18**, 572–585 (2008).
3. C. Cuesta, C. Arévalo-Alameda, E. Castellano, The importance of being PI3K in the RAS signaling network. *Genes* **12**, 1094 (2021).
4. N. Özören, W. S. El-Deiry, Cell surface death receptor signaling in normal and cancer cells. *Semin. Cancer Biol.* **13**, 135–147 (2003).
5. K. Cho, J. I. Joo, D. Shin, D. Kim, S. Park, The reverse control of irreversible biological processes. *Wiley Interdiscip. Rev. Syst. Biol. Med.* **8**, 366–377 (2016).
6. R.-S. Wang, A. Saadatpour, R. Albert, Boolean modeling in systems biology: An overview of methodology and applications. *Phys. Biol.* **9**, 055001 (2012).
7. M. Choi, J. Shi, S. H. Jung, X. Chen, K.-H. Cho, Attractor landscape analysis reveals feedback loops in the p53 network that control the cellular response to DNA damage. *Sci. Signal.* **5**, ra83 (2012).
8. M. Choi, J. Shi, Y. Zhu, R. Yang, K.-H. Cho, Network dynamics-based cancer panel stratification for systemic prediction of anticancer drug response. *Nat. Commun.* **8**, 1940 (2017).
9. J. Kim, S.-M. Park, K.-H. Cho, Discovery of a kernel for controlling biomolecular regulatory networks. *Sci. Rep.* **3**, 2223 (2013).
10. S.-M. Choo, B. Ban, J. I. Joo, K.-H. Cho, The phenotype control kernel of a biomolecular regulatory network. *BMC Syst. Biol.* **12**, 49 (2018).
11. J. G. Zanudo, R. Albert, Cell fate reprogramming by control of intracellular network dynamics. *PLoS Comput. Biol.* **11**, e1004193 (2015).
12. G. Yang, J. G. T. Zañudo, R. Albert, Target control in logical models using the domain of influence of nodes. *Front. Physiol.* **9**, 454 (2018).
13. N. Kim, J. Lee, J. Kim, Y. Kim, K.-H. Cho, Canalizing kernel for cell fate determination. *Brief. Bioinform.* **25**, bbae406 (2024).
14. N. Kim, C. Y. Hwang, T. Kim, H. Kim, K.-H. Cho, A cell-fate reprogramming strategy reverses epithelial-to-mesenchymal transition of lung cancer cells while avoiding hybrid states. *Cancer Res.* **83**, 956–970 (2023).
15. S. R. Choi, C. Y. Hwang, J. Lee, K.-H. Cho, Network analysis identifies regulators of basal-like breast cancer reprogramming and endocrine therapy vulnerability. *Cancer Res.* **82**, 320–333 (2022).

16. S. An, S.-Y. Cho, J. Kang, S. Lee, H.-S. Kim, D.-J. Min, E. Son, K.-H. Cho, Inhibition of 3-phosphoinositide–dependent protein kinase 1 (PDK1) can revert cellular senescence in human dermal fibroblasts. *Proc. Natl. Acad. Sci. U.S.A.* **117**, 31535–31546 (2020).
17. J. I. Joo, H. Park, K. Cho, Normalizing input–output relationships of cancer networks for reversion therapy. *Adv. Sci.* **10**, 2207322 (2023).
18. H. Li, L. Xie, Y. Wang, Output Regulation of Boolean Control Networks. *IEEE Trans Automat Contr* **62**, 2993–2998 (2017).
19. H. Li, Y. Wang, Output feedback stabilization control design for Boolean control networks. *Automatica* **49**, 3641–3645 (2013).
20. J.-M. Yang, C.-K. Lee, K.-H. Cho, output stabilizing control of complex biological networks based on Boolean algebra analysis. *IEEE Trans. Neural Netw. Learn Syst.* **36**, 9210–9223 (2025).
21. D. Shin, J.-R. Gong, S. D. Jeong, Y. Cho, H.-P. Kim, T.-Y. Kim, K.-H. Cho, Attractor landscape analysis reveals a reversion switch in the transition of colorectal tumorigenesis. *Adv. Sci.* **12**, 2412503 (2025).
22. J.-R. Gong, C.-K. Lee, H.-M. Kim, J. Kim, J. Jeon, S. Park, K.-H. Cho, Control of cellular differentiation trajectories for cancer reversion. *Adv. Sci.* **12**, 2402132 (2025).
23. J. Zhong, Y. Liu, K. I. Kou, L. Sun, J. Cao, On the ensemble controllability of Boolean control networks using STP method. *Appl. Math Comput.* **358**, 51–62 (2019).
24. A. Yerudkar, C. Del Vecchio, L. Glielmo, Output tracking control design of switched Boolean control networks. *IEEE Control Syst. Lett.* **4**, 355–360 (2020).
25. H. Liu, Y. Liu, Y. Li, Z. Wang, F. E. Alsaadi, Observability of Boolean networks via STP and graph methods. *IET Control Theory Appl* **13**, 1031–1037 (2019).
26. A. Rushdi, F. Muhammad Ghaleb, A tutorial exposition of semi-tensor products of matrices with a stress on their representation of Boolean functions. *JKAU: Comp. Sci.* **5**, 3–30 (2016).
27. Y. Wang, Y. Yang, Y. Liu, J. Lou, Fault detection and pinning control of Boolean networks. *Appl. Math Comput.* **429**, 127232 (2022).
28. J. Lu, H. Li, Y. Liu, F. Li, Survey on semi-tensor product method with its applications in logical networks and other finite-valued systems. *IET Control Theory Appl* **11**, 2040–2047 (2017).
29. J. C. Rozum, J. Gómez Tejeda Zañudo, X. Gan, D. Deritei, R. Albert, Parity and time reversal elucidate both decision-making in empirical models and attractor scaling in critical Boolean networks. *Sci. Adv.* **7**, eabf8124 (2021).
30. D. J. Irons, Improving the efficiency of attractor cycle identification in Boolean networks. *Phys. D: Nonlinear Phenom.* **217**, 7–21 (2006).
31. T. Parmer, L. M. Rocha, F. Radicchi, Influence maximization in Boolean networks. *Nat. Commun.* **13**, 3457 (2022).
32. Ö. Sahin, H. Fröhlich, C. Löbke, U. Korf, S. Burmester, M. Majety, J. Mattern, I. Schupp, C. Chaouiya, D. Thieffry, A. Poustka, S. Wiemann, T. Beissbarth, D. Arlt, Modeling ERBB receptor-regulated G1/S transition to find novel targets for de novo trastuzumab resistance. *BMC Syst. Biol.* **3**, 1 (2009).
33. M. E. Martinez-Sanchez, L. Huerta, E. R. Alvarez-Buylla, C. Villarreal Luján, Role of cytokine combinations on CD4+ T cell differentiation, partial polarization, and plasticity: Continuous network modeling approach. *Front. Physiol.* **9**, 877 (2018).
34. B. Offermann, S. Knauer, A. Singh, M. L. Fernández-Cachón, M. Klose, S. Kowar, H. Busch, M. Boerries, Boolean modeling reveals the necessity of transcriptional regulation for bistability in PC12 cell differentiation. *Front. Genet.* **7**, 44 (2016).
35. S. Collombet, C. van Oevelen, J. L. Sardina Ortega, W. Abou-Jaoudé, B. Di Stefano, M. Thomas-Chollier, T. Graf, D. Thieffry, Logical modeling of lymphoid and myeloid cell specification and transdifferentiation. *Proc. Natl. Acad. Sci. U.S.A.* **114**, 5792–5799 (2017).
36. P. Bloomingdale, V. A. Nguyen, J. Niu, D. E. Mager, Boolean network modeling in systems pharmacology. *J. Pharmacokinet. Pharmacodyn.* **45**, 159–180 (2018).
37. X. F. Wang, G. Chen, Complex networks: small-world, scale-free and beyond. *IEEE Circuits Syst. Mag.* **3**, 6–20 (2003).
38. C. Kadelka, T.-M. Butrie, E. Hilton, J. Kinseth, A. Schmidt, H. Serdarevic, A meta-analysis of Boolean network models reveals design principles of gene regulatory networks. *Sci. Adv.* **10**, eadj0822 (2024).
39. A. Ghavasieh, M. De Domenico, Diversity of information pathways drives sparsity in real-world networks. *Nat. Phys.* **20**, 512–519 (2024).
40. C. Kadelka, D. Murrugarra, Canalization reduces the nonlinearity of regulation in biological networks. *npj Syst. Biol. Appl.* **10**, 67 (2024).
41. K. Kobayashi, Design of fixed points in Boolean networks using feedback vertex sets and model reduction. *Complexity* **2019**, 9261793 (2019).
42. S. An, S.-Y. Jang, S.-M. Park, C.-K. Lee, H.-M. Kim, K.-H. Cho, Global stabilizing control of large-scale biomolecular regulatory networks. *Bioinformatics* **39**, btad045 (2023).
43. L. Grieco, L. Calzone, I. Bernard-Pierrot, F. Radvanyi, B. Kahn-Perlès, D. Thieffry, Integrative modelling of the influence of MAPK network on cancer cell fate decision. *PLoS Comput. Biol.* **9**, e1003286 (2013).
44. B. D. Hopkins, C. Hodakoski, D. Barrows, S. M. Mense, R. E. Parsons, PTEN function: The long and the short of it. *Trends Biochem. Sci.* **39**, 183–190 (2014).
45. M. S. Song, L. Salmena, P. P. Pandolfi, The functions and regulation of the PTEN tumour suppressor. *Nat. Rev. Mol. Cell Biol.* **13**, 283–296 (2012).
46. A. Krohn, T. Diedler, L. Burkhardt, P.-S. Mayer, C. De Silva, M. Meyer-Kornblum, D. Kötschau, P. Tennstedt, J. Huang, C. Gerhäuser, M. Mader, S. Kurtz, H. Sirma, F. Saad, T. Steuber, M. Graefen, C. Plass, G. Sauter, R. Simon, S. Minner, T. Schlomm, Genomic deletion of *PTEN* is associated with tumor progression and early PSA recurrence in ERG fusion-positive and fusion-negative prostate cancer. *Am. J. Pathol.* **181**, 401–412 (2012).
47. P. Cairns, E. Evron, K. Okami, N. Halachmi, M. Esteller, J. G. Herman, S. Bose, S. I. Wang, R. Parsons, D. Sidransky, Point mutation and homozygous deletion of PTEN/MMAC1 in primary bladder cancers. *Oncogene* **16**, 3215–3218 (1998).
48. S. Hara, M. Oya, R. Mizuno, A. Horiguchi, K. Marumo, M. Murai, Akt activation in renal cell carcinoma: contribution of a decreased PTEN expression and the induction of apoptosis by an Akt inhibitor. *Ann. Oncol.* **16**, 928–933 (2005).
49. J. Saez-Rodriguez, L. Simeoni, J. A. Lindquist, R. Hemenway, U. Bommhardt, B. Arndt, U.-U. Haus, R. Weismantel, E. D. Gilles, S. Klamt, B. Schraven, A logical model provides insights into T cell receptor signaling. *PLoS Comput. Biol.* **3**, e163 (2007).
50. K. W. Wucherpfennig, P. Höllsberg, J. H. Richardson, D. Benjamin, D. A. Hafler, T-cell activation by autologous human T-cell leukemia virus type I-infected T-cell clones. *Proc. Natl. Acad. Sci. U.S.A.* **89**, 2110–2114 (1992).
51. H. Suzuki, T. M. Kündig, C. Furlonger, A. Wakeham, E. Timms, T. Matsuyama, R. Schmits, J. J. L. Simard, P. S. Ohashi, H. Griesser, T. Taniguchi, C. J. Paige, T. W. Mak, Deregulated T cell activation and autoimmunity in mice lacking interleukin-2 receptor β. *Science* **268**, 1472–1476 (1995).
52. R. L. Wange, LAT, the linker for activation of T cells: A bridge between T cell-specific and general signaling pathways. *Sci. STKE* **2000**, re1 (2000).
53. M. Karin, The regulation of AP-1 activity by mitogen-activated protein kinases. *J. Biol. Chem.* **270**, 16483–16486 (1995).
54. A. J. Whitmarsh, R. J. Davis, Transcription factor AP-1 regulation by mitogen-activated protein kinase signal transduction pathways. *J. Mol. Med.* **74**, 589–607 (1996).
55. R. Khanin, E. Wit, How scale-free are biological networks. *J. Comput. Biol.* **13**, 810–818 (2006).
56. E. Wong, B. Baur, S. Quader, C.-H. Huang, Biological network motif detection: principles and practice. *Brief. Bioinform.* **13**, 202–215 (2012).

Acknowledgments

Funding: This work was supported by the National Research Foundation of Korea (NRF) grants funded by the Korea Government, the Ministry of Science and ICT (RS-2023-NR077224, RS-2024-00405360 and RS-2025-17652976), and the Bio & Medical Technology Development Program of NRF funded by the Ministry of Science and ICT (2021M3A9I4024447). This research was also supported by a grant of the Korea Dementia Research Project through the Korea Dementia Research Center (KDRC), funded by the Ministry of Health & Welfare and Ministry of Science and ICT, Republic of Korea (grant number RS-2025-02264017). **Author contributions:** I.J. and K.-H.C. conceived the study and designed an algebraic framework. I.J. conduced computational simulations and developed the algorithm. C.H., S.H.-J., and H.Y. provided analytic and technical supports. K.-H.C., I.J., and C.H. wrote the manuscript. K.-H.C. designed the project and supervised the research. **Competing interests:** The authors declare that they have no competing interests. **Data and materials availability:** All data needed to evaluate the conclusions of the paper are present in the paper and/or the Supplementary Materials. Code and data have been deposited in Zenodo and are publicly available at https://doi.org/10.5281/zenodo.15532673 and at our GitHub repository (https://github.com/Insoo-Jung/Phenotype-Landscape-Reversion).

Submitted 30 January 2025
Accepted 21 July 2025
Published 22 August 2025
10.1126/sciadv.adw3995

Science Advances

Reverse control of biological networks to restore phenotype landscapes

Insoo Jung, Corbin Hopper, Seong-Hoon Jang, Hyunsoo Yeo, and Kwang-Hyun Cho

Sci. Adv. **11** (34), eadw3995. DOI: 10.1126/sciadv.adw3995

Science Advances (ISSN 2375-2548) is published by the American Association for the Advancement of Science. 1200 New York Avenue NW, Washington, DC 20005. The title *Science Advances* is a registered trademark of AAAS.